

A Cantilever Torque Magnetometry Method for the Measurement of Hall Conductivity of Highly Resistive Samples

Samuel Mumford,^{1,2} Tiffany Paul,^{1,3} Seung Hwan Lee,⁴ Amir Yacoby,⁴ and Aharon Kapitulnik^{1,2,3}

¹*Geballe Laboratory for Advanced Materials, Stanford University, Stanford CA, 94305, USA*

²*Department of Physics, Stanford University, Stanford CA, 94305, USA*

³*Department of Applied Physics, Stanford University, Stanford CA, 94305, USA*

⁴*Department of Physics, Harvard University, Cambridge MA, 02138, USA*

(Dated: May 6, 2022)

We present the first measurements of Hall conductivity utilizing a new torque magnetometry method designed for insulators. A Corbino disk exhibits a magnetic dipole moment proportional to Hall conductivity when voltage is applied across a test material. This magnetic dipole moment can be measured through torque magnetometry. The symmetry of this contactless technique allows for the measurement of Hall conductivity in previously inaccessible materials. Finally, a low-temperature noise bound, the lack of systematic errors on dummy devices, and a measurement of the Hall conductivity of sputtered indium tin oxide demonstrate the efficacy of the technique.

I. INTRODUCTION

Measurements of transverse transport properties such as the Hall effect, Nernst effect, and transverse thermal conductivity have become of great importance in understanding modern quantum materials. However, such measurements are often made difficult, or even impossible, due to contamination of longitudinal transport effects. For example, in a standard Hall bar measurement of the Hall effect, the transverse voltage $V_y(H)$ is measured in response to the application of a longitudinal current I_x in the presence of a perpendicular magnetic field $H\hat{z}$ using two contacts on opposite sides of the sample (see Fig. 1a). A common procedure to eliminate contributions from the longitudinal magnetoresistance due to contact misalignment invokes the odd symmetry of the effect to find Hall resistance $\rho_{xy} = [V_y(H) - V_y(-H)]/2I_x$. Here we use 2D notation where thickness is fixed. However, this simple procedure often fails when $\rho_{xx} \gg \rho_{xy}$, as is the case in the variable range hopping (VRH) regime of disordered insulators [1, 2], or on the insulating side of superconductor-insulator transition [3–7]. Similarly, only a handful of Hall measurements were done in the VRH regime (see e.g. [8, 9]) despite detailed theories [10, 11], and in general measurements were restricted to the vicinity of the metal-insulator transition. The issue is further amplified if one is interested in the transverse conductivity σ_{xy} , which can be calculated from the resistivity tensor, but with uncontrolled error-bars if ρ_{xx} diverges. A direct measurement of σ_{xy} is also needed to probe a variety of topological states of matter in the bulk of the material-system where edge states may dominate the transport. For example, standard transport approaches to measure the quantum Hall effect (QHE) in two dimensional electron gas (2DEG) interact directly with the edge states, with no ability to explore the existence of Hall currents in the bulk of the sample [12]. Indeed, the original theoretical approach to explain the QHE by Laughlin [13] used a closed metallic ribbon configuration, equivalent to a Corbino disk [14], to demonstrate the effect.

In this paper we demonstrate a new method for measuring σ_{xy} in a Corbino disk configuration, where the induced Hall currents in the disk create a magnetic dipole that is

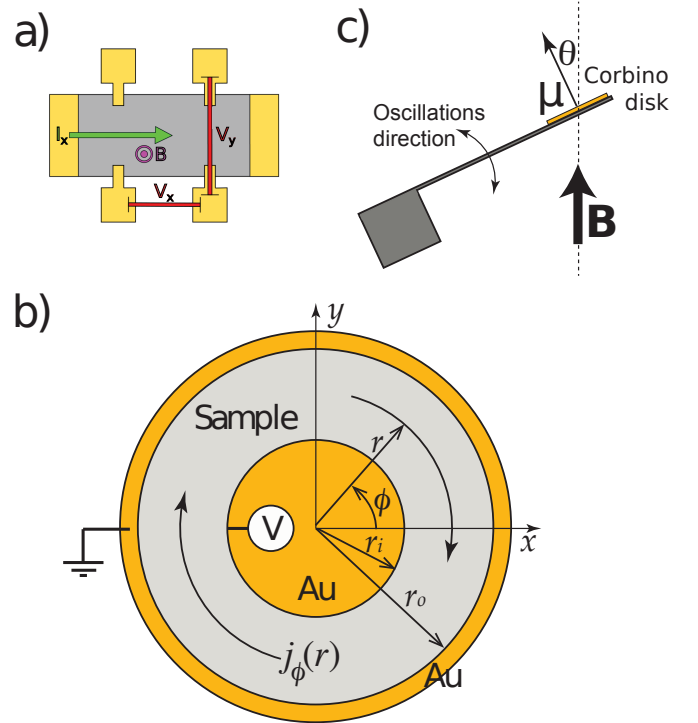


FIG. 1. a) The typical Hall bar consists of four contacts and a drive current I . A symmetry-breaking magnetic field B allows for a non-diagonal terms in the resistivity tensor ρ . Correspondingly, there is a Hall voltage $V_{xy} \propto \rho_{xy}I_x$ across contacts separated \perp to I_x as well as the longitudinal voltage $V_{xx} \propto \rho_{xx}I_x$. b) Corbino disk configuration used for σ_{xy} measurements. Here the Au metallic contacts serve as the equipotential rings. c) Side view of torque magnetometry.

measured by torque magnetometry. A circularly symmetric Corbino disk is shown in Fig. 1b. Fabricated at the end of a cantilever, it forms the basis of this σ_{xy} measurement technique [14]. Applying a voltage V between the inner and outer contacts creates a radial electric field E_r , which induces a circulating Hall current with a current density $j_\phi(r)$. These Hall currents create a magnetic dipole moment μ parallel to the

ring normal, which can be directly evaluated by

$$\mu = \int j_\phi(r) \pi r^2 dr = \int \sigma_{xy} E_r \pi r^2 dr \equiv \sigma_{xy} G V \quad (1)$$

where G is a geometrical factor. For concentric rings one obtains

$$\mu = \sigma_{xy} \frac{\pi(r_o^2 - r_i^2)}{2 \ln(r_o/r_i)} V \quad (2)$$

where r_i and r_o are the inner and outer radii of the test material respectively. While real fabricated devices may deviate slightly from concentric rings, an image of the device can be used to numerically correct for that error.

The magnetic dipole moment is then measured by means of torque magnetometry as shown in Fig. 1c, which allows for a high-precision contactless measurement. The dipole moment is measured without placing elements in series with the Hall current, and the torque measurement is insensitive to higher order magnetic moments caused by misalignment. The magnetic dipole moment of the full Corbino disk is also relatively insensitive to local disorder sources. Moreover, as the Corbino disk torque must be linear in V and even in B , one may separate the signal due to the Hall effect from other effects due to cantilever heating or longitudinal current by signal symmetry.

II. METHODS

A. Measurement Concept

Cantilever torque magnetometry utilizes a high- Q resonator to detect the interaction between a magnetic dipole and an external magnetic field [15–17]. The angular response θ of a cantilever with moment of inertia A , resonant frequency $\omega_0 = 2\pi f_0$, and quality factor Q subject to an external torque τ may be approximated as a damped harmonic oscillator following [18]

$$I\ddot{\theta} + QA\omega_0\dot{\theta} + A\omega_0^2\theta = \tau. \quad (3)$$

An external magnetic field \vec{B} exerts a torque [15]

$$\vec{\tau} = \vec{\mu} \times \vec{B}. \quad (4)$$

If the dipole moment and magnetic field are aligned in the cantilever equilibrium position, an effective detuning torque

$$\tau_D = \mu B \sin(\theta) \approx \mu B \theta \quad (5)$$

results as the cantilever oscillates. Inserting τ_D into Equation 3 shifts the resonant frequency by

$$A\omega_0^2 \rightarrow A\omega_0^2 - \mu B, \quad \text{or} \quad \frac{\Delta\omega_0}{\omega_0} = \frac{\mu B}{2A\omega_0^2}. \quad (6)$$

Using Eqn. 2, the shift in resonant frequency can be related to the applied voltage, magnetic field, and σ_{xy} by

$$\delta f_0 = \frac{GV}{8\pi^2 A f_0} B \sigma_{xy}. \quad (7)$$

Measurement of changes in f_0 of a patterned cantilever with voltage therefore probes σ_{xy} without polluting terms from ρ_{xx} .

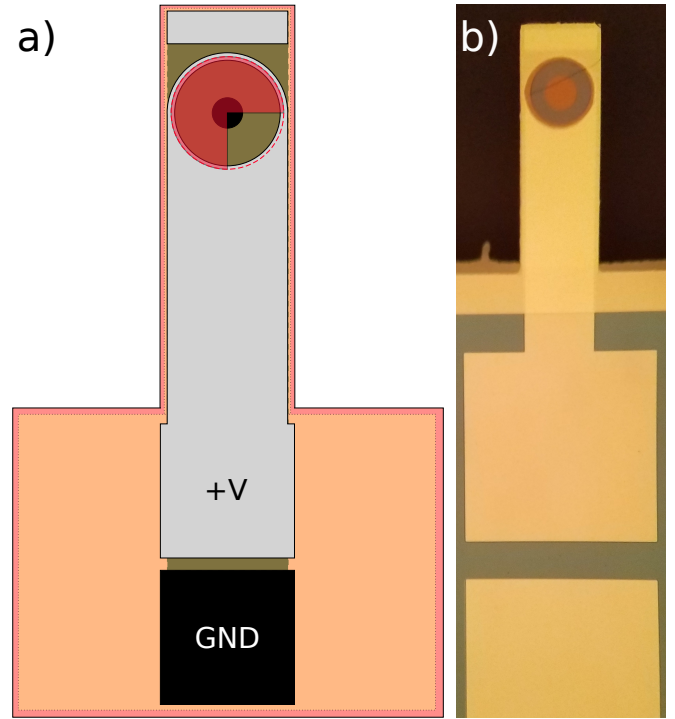


FIG. 2. a) Schematic drawing of a cantilever patterned with a Corbino disk in the planar coaxial design. An insulating barrier (orange) separates the Pt inner contact (black) and the Pt outer ring contact (gray). The test material (red) is deposited in a circle connecting the voltage contacts. b) A planar coaxial Corbino disk cantilever with ITO as the test material.

B. Device Fabrication

Corbino disks were patterned on high- Q single-crystal silicon cantilevers as shown in Fig. 2. Fabrication was performed using photolithography as all features are larger than $15 \mu\text{m}$. Fabrication began with a silicon on insulator (SOI) wafer with a $450 \mu\text{m}$ handle layer, a $4 \mu\text{m}$ buried oxide layer, and a 2 or $3 \mu\text{m}$ device layer of (001) Si depending on the design. A CVD SiO_2 layer was first deposited onto the handle side and this oxide was plasma etched in an array of square windows. Next, 25 nm of Ti-Pt was patterned in the shape of the cantilever on the device side. This conductive layer serves as a ground plane and separates the Corbino disk voltages from the underlying Si. A 40 nm thick barrier of ALD HfO_2 and CVD nitride were then grown on top of the Pt to electrically separate the grounding plane from subsequently deposited layers. On the planar coaxial design shown in Fig. 2, a hole was etched in this insulating layer for the grounded central Corbino disk contact and the Pt outer contact was deposited directly onto the SiN- HfO_2 insulating layer. The ground plane serves both as the inner contact and as a conductive barrier in the planar coaxial design. The cantilever shape was etched out from the device layer Si using a Bosch etcher. Finally, the test material was deposited between the inner and outer contacts and the cantilever was released using a backside Bosch etch and a final oxide plasma etch.

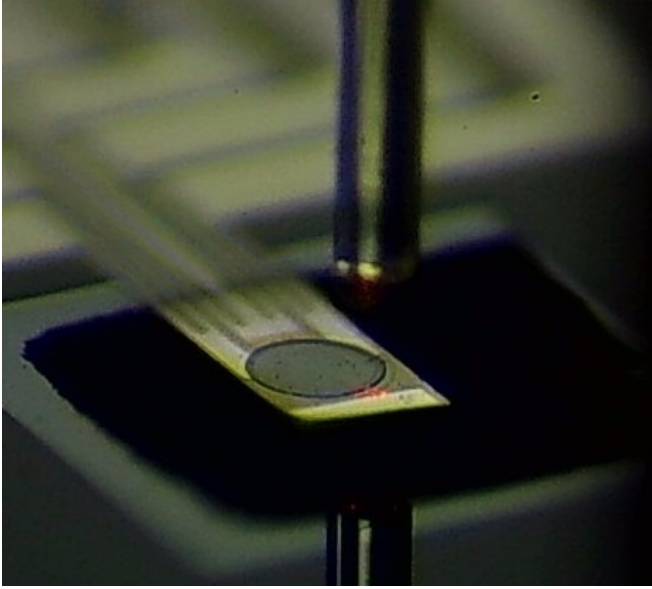


FIG. 3. A cleaved fiber above a cantilever forming an interferometer. The two interfering light sources are reflected light from the fiber end and the cantilever surface. The fiber was aligned with a three-axis stage and a red laser before being epoxied to the cantilever wafer. A separate pad of Pt was patterned on the end of the cantilever for alignment.

For devices with separate grounded wires on top of the ground plane, such as the Ge dummy device of Section III B, the SiN-HfO₂ insulating barrier was not etched. A thin Ti-Au inner contact was instead deposited onto this insulating substrate and a 20 nm thick ALD HfO₂ ring was patterned to cover most of this inner contact. This ring separates the inner and outer voltage contacts. The resulting cantilevers with separate ground planes are 250 μm x 600 μm x 3 μm and $f_0 \sim 10$ kHz. The planar coaxial design cantilevers are 200 μm x 600 μm x 2 μm and with $f_0 \sim 7$ kHz. Both exhibit $Q \sim 25000$ at pressures below 1×10^{-4} Torr.

C. Interferometric Resonant Frequency Detection

The resonant frequency of the cantilever is tracked with a fiber interferometer. The output of a 1310 nm fiber-coupled laser diode is first fed through a 90-10 splitter. The majority of the laser power goes to a reference photodiode and the remaining 10% of laser power is connected to a cleaved fiber optic cable. The cleaved fiber end is then aligned over a cantilever to form an interferometer as shown in Fig. 3. The output from this interferometer is converted into a voltage by a photodiode and computer processed after analog-to-digital conversion. The interferometer voltage $V(t)$ for laser wavelength λ , peak to peak voltage V_{pp} , and fiber-cantilever distance Δz is

$$V(t) \approx \frac{2\pi V_{pp} \Delta z(t)}{\lambda} \sin\left(\frac{4\pi \Delta z_0}{\lambda}\right) \propto \Delta z(t). \quad (8)$$

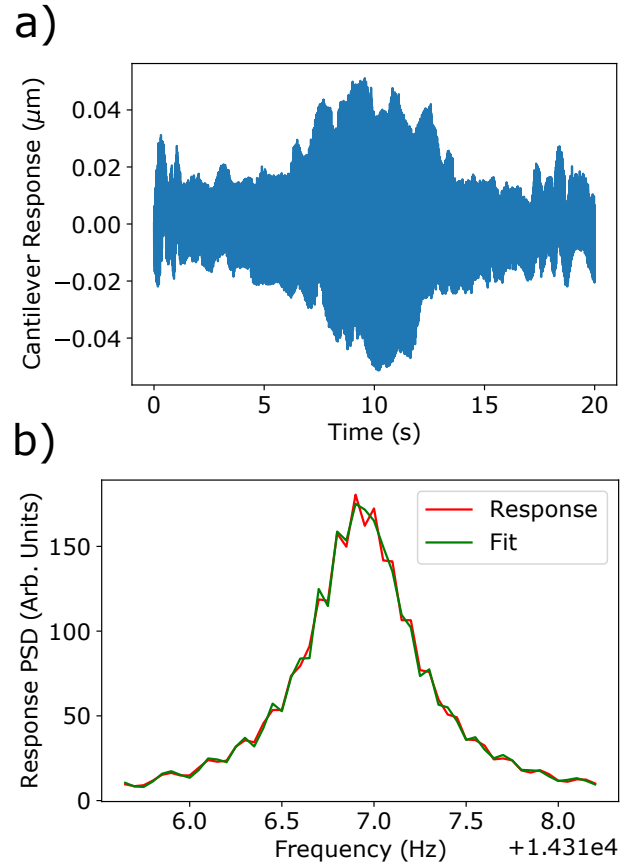


FIG. 4. a) Real time response of a 3 μm thick Si cantilever to a sweep drive. The amplitude of driving power modulation was 50 μW. Each drive and fit was performed over 20 s so subsequent drives would be independent with a cantilever response time of ~ 2 s. b) Power spectral density of the cantilever response seen in part a. Response is fit to a damped harmonic oscillator equation.

The fiber interferometer thus provides the means to precisely track cantilever motion.

Cantilever resonant frequency is measured by observing the response to a radiation pressure drive. A 1550 nm fiber coupled laser is connected to the cleaved fiber used for interferometry. The power of this laser is reflected off of a Pt pad near the end of the cantilever. This laser power is modulated with a frequency sweeping voltage over a frequency width δf and time t_{sw}

$$V_{sw} = V_0 \sin\left[2\pi\left(f_0 - \frac{\delta f}{2} + \frac{\delta f t}{2t_{sw}}\right)t\right] \quad (9)$$

to create a sweeping radiation pressure drive. The sweeping drive voltage is also connected to a reference port in the analog-to-digital converter to fit for the cantilever response function, shown in Fig. 4.

As shown in Appendix A, the minimum detectable shift in resonant frequency for a cantilever with length L and vibra-

tional temperature T driven for time t_{samp} is

$$\frac{\Delta\omega_0}{\omega_0} = \frac{2L}{\lambda} \sqrt{\frac{2k_b T \pi}{A\omega_0^3 t_{samp} Q}}, \quad (10)$$

which by Equations 2 and 6 translates to a minimum detectable σ_{xy} of

$$\delta\sigma_{xy} = \frac{4L \ln(r_o/r_i)}{\lambda(r_o^2 - r_i^2)VB} \sqrt{\frac{2k_b T A \omega_0}{\pi t_{samp} Q}}. \quad (11)$$

For this cantilever design, dilution refrigerator temperature of 0.1 K, a 1 T magnet, and 0.1 V applied, the minimum detectable $\sigma_{xy} \sim 10^{-9} \Omega^{-1}$. Such uncertainty improves upon Hall bar measurements for insulating samples extrapolated to $T \rightarrow 0$ by a factor of $> 10^5$ [19]. Note as sample heating scales as V^2/ρ , the minimum observable σ_{xy} scales as $1/\sqrt{\rho}$ and decreases dramatically for insulators at low temperature.

III. EXPERIMENTAL RESULTS

A. Systematics Tests: Conductive Pt Device

Dummy devices without Corbino disks were investigated to check for systematic errors which could create a shift in f_0 similar to a Hall signal. An initial dummy device consisted of Pt wires and a ground plane patterned on a $3 \mu\text{m}$ thick single-crystal Si cantilever, shown in Fig. 5a. The resistance of the Pt wires was 850Ω , and alternating voltages $V = \pm 350 \text{ mV}$ were applied across the device to look for an odd in V and even in B shift in f_0 . The observed shift in f_0 at room temperature between $\pm V$, $f_0(+V) - f_0(-V)$ or δf_0 , is $-4 \pm 26 \mu\text{Hz}$. A second Pt dummy cantilever was tested at room temperature and similarly displays $\delta f_0 = 29 \pm 28 \mu\text{Hz}$. The grounded Pt cantilevers thus show no evidence of a zero-field δf_0 as expected. The Pt dummy was also cooled to 4.2 K and exposed to $\pm 1 \text{ T}$ of magnetic field in a Janis SVT cryostat. The sum of δf_0 for $\pm B$ is $0.27 \pm 0.21 \text{ mHz}$ and the zero field δf_0 at 4.2 K is $-0.03 \pm 0.1 \text{ mHz}$. The Pt dummy cantilevers thus demonstrate no evidence of a zero-field or Hall-like δf_0 at both room temperature and liquid helium temperature.

B. Systematics Tests: Insulating Ge Device

Full Corbino disk cantilevers with evaporated amorphous Ge as a test material were also fabricated (Fig. 5b). The insulating Ge serves both as a test for spurious δf_0 with voltage applied across the ring and as a means to verify that the full fabrication procedure did not create unintended electrical connections. The $3 \mu\text{m}$ thick Ge devices are both electrically and mechanically viable, with resistances of $> 20 \text{ M}\Omega$ and $Q \sim 25000$. Once more, there is no evidence of a Hall-like shift in f_0 at room temperature, finding $\delta f_0 = 88 \pm 91 \mu\text{Hz}$ in 0 field and $\delta f_0 = 30 \pm 80 \mu\text{Hz}$ above a 0.3 T static magnet.

In conclusion, the dummy device tests demonstrate that design flaws creating Hall-like δf_0 have been eliminated. Hall

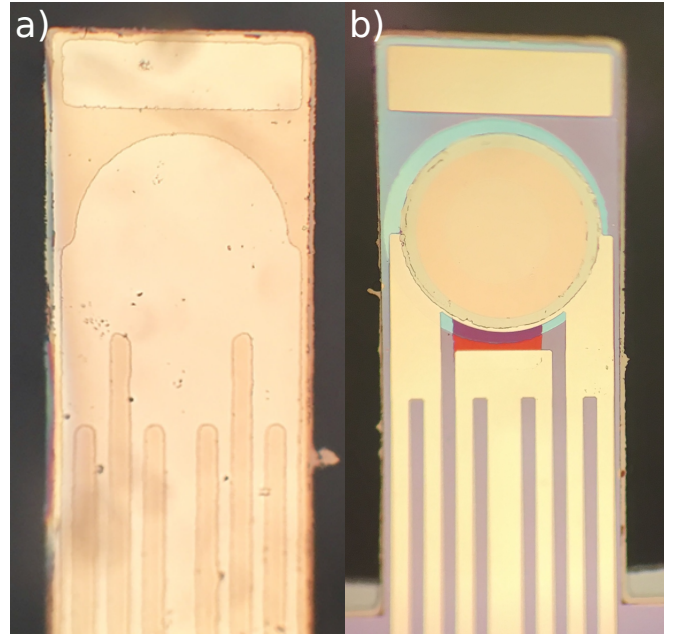


FIG. 5. a) A dummy device with Pt wires used to look for systematic errors and noise bounds. b) A Corbino disk cantilever with Ge as a test material. Note the pairs of wires for the inner and outer contacts to allow for four wire measurement of the voltage across the disk.

signal therefore may be distinguished by voltage and magnetic field behavior from other shifts in f_0 in patterned Si cantilevers with Corbino disks.

C. Measurements of ITO Corbino Disk

Corbino cantilevers with indium tin oxide (ITO) as a sample material were fabricated for first measurements of Hall signal. ITO was chosen as an example of a disordered itinerant system which can be tuned through a metal-insulator transition (MIT) by changing the tin and oxygen content. Here we sputtered 50 nm of ITO with resistivity $3.5 \times 10^{-3} \Omega\text{-cm}$. Such ITO should exhibit $\sigma_{xy} > 1 \times 10^{-7} \Omega^{-1}$ at 5 T [20]. Based on the observed carrier density in this system such ITO should be in the vicinity of the MIT with $k_F \ell \lesssim 1$. With typical carrier density for this material, it is expected that $\rho_{xy}/\rho_{xx} \sim 10^{-5}$ which is on the borderline of standard methods of Hall effect detection[20].

Cantilevers with ITO Corbino disks were tested to verify a real Hall signal can be seen. In an effort to improve future torque sensitivity, thinner $2 \mu\text{m}$ thick planar coaxial cantilevers were fabricated as shown in Fig. 2. Fig. 6 shows $\delta f_0(B)$ of a cantilever in two datataking runs at 4.2 K. After fitting to a second order polynomial and subtracting the linear component, the Hall signal of the ITO can clearly be observed as a quadratic dependence in $\delta f_0(B)$ in Fig. 7. This quadratic dependence is seen in both datataking runs, yielding fit coefficients of $29.2 \pm 4.6 \mu\text{Hz/T}^2$ and $47.1 \pm 9.3 \mu\text{Hz/T}^2$. The order of datataking was reversed for the second run, confirming that the quadratic dependence in $\delta f_0(B)$ is not a tem-

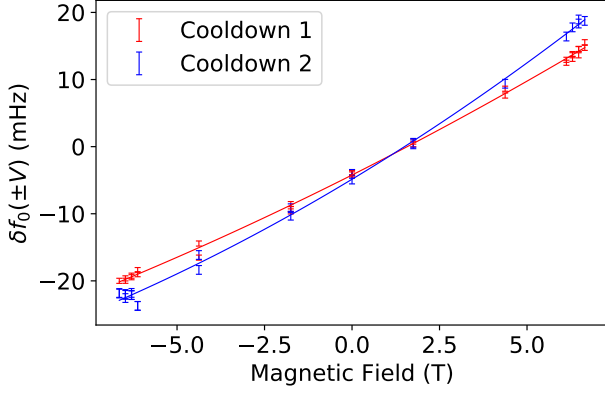


FIG. 6. Data and fit for $\delta f_0(B)$ with ± 0.1 V applied across the device. Note the overriding linear dependence due to patterning asymmetry of the current-carrying Pt wires. This can be used to compare A between cooldowns on the same cantilever.

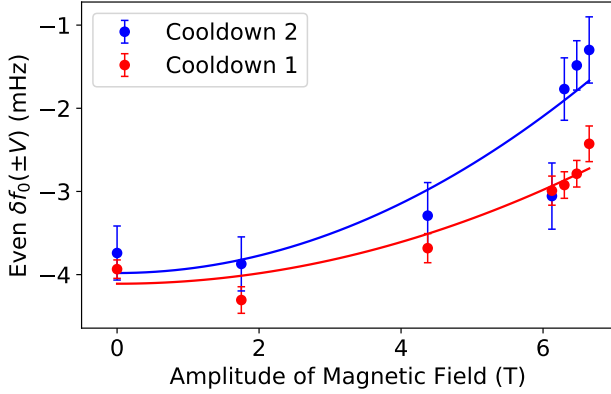


FIG. 7. Data and quadratic fit for the even component of $\delta f_0(B)$. There is a clear quadratic Hall signal in all cooldowns with sputtered ITO as a test material.

perature or time effect. A second cantilever from the same wafer was tested to confirm that the curvature of $\delta f_0(B)$ could be attributed to the ITO. On the second device the curvature in $\delta f_0(B)$ is $46.7 \pm 8.7 \mu\text{Hz}/\text{T}^2$. Using Eqn. 7, at 5 T the quadratic fit coefficient of each cantilever translates to σ_{xy} of $(2.33 \pm 0.40) \times 10^{-7} \Omega^{-1}$ and $(2.21 \pm 0.42) \times 10^{-7} \Omega^{-1}$. Converting back to resistivities, $\rho_{xy} \sim 0.1 \Omega$ or $5 \times 10^{-7} \Omega\text{-cm}$ in 3D units. This statistically consistent result for σ_{xy} across different cantilevers, cooldowns, and data taking procedures is in agreement with previous measurements of sputtered ITO and verifies that the observed quadratic dependence in $\delta f_0(B)$ is caused by the ITO Corbino disk. The small ratio of ρ_{xy}/ρ_{xx} also demonstrates the effectiveness of the technique.

IV. SUMMARY

In conclusion, Corbino disk torque magnetometry is a viable method for measuring σ_{xy} . First, the initial challenge of fabricating high- Q cantilevers with patterned Corbino disks and contacts has been completed. The resonant frequency of such devices can be measured with a fractional uncertainty of less than one part in 10^7 , even in conditions that have not yet employed vibration isolation, high vacuum conditions, or special shielding. The Corbino disk cantilevers have also been tested for errors in fabrication, data collection procedures, and analysis protocols. This allowed for the elimination of systematic errors and spurious signals, both when applying current and voltage across the disk. These new cantilevers have also been used to measure σ_{xy} of sputtered ITO with nominal resistivity of $\rho_{xx} \sim 3.5 \times 10^{-3} \Omega\text{-cm}$, demonstrating the ability to detect the Hall effect in samples where $\rho_{xy}/\rho_{xx} \sim 10^{-5}$ [20], which is generally difficult to measure using standard techniques.

ACKNOWLEDGMENTS

This work was funded by the Army Research Office grant W911NF1710588, and by the Gordon and Betty Moore Foundation through Emergent Phenomena in Quantum Systems (EPiQS) Initiative Grant GBMF4529. This work was also funded in part by a QuantEmX grant from ICAM and the Gordon and Betty Moore Foundation through Grant GBMF5305 to Seung Hwan Lee.

Appendix A: Theoretical Noise Floor Calculation

For a cantilever response function $R(\omega, \omega_0)$ to an applied torque τ_{app} , the observed change in cantilever oscillation when the resonant frequency shifts by $\Delta\omega_0$ is

$$\Delta\theta_{sig}(\omega) = \tau_{app}(\omega) \frac{dR}{d\omega_0} \Delta\omega_0.$$

As seen in Fig. 4a, τ_{app} is limited by interferometer wavelength λ . For a cantilever of length L the maximum angle of deflection over time t_{samp} is

$$\Delta\theta_{max} = \lambda/2L = \tau_{max}(\omega)R(\omega)2\pi/t_{samp}.$$

The largest possible signal for a single-frequency drive therefore is

$$\Delta\theta_{sig}(\omega) = \frac{\lambda t_{samp}}{2L} \frac{dR}{d\omega_0} \frac{1}{R(\omega)} \Delta\omega_0.$$

The fundamental experimental noise source is thermal vibration. By equipartition $k_B T = A \langle \theta^2(t) \rangle$, or assuming a white noise thermal drive τ_{therm}

$$\langle \theta^2(t) \rangle = \frac{\tau_{therm}^2}{t_{samp}} \int R^2(\omega) d\omega = \frac{k_B T}{A}.$$

So with

$$\tau_{therm}(\omega) = \sqrt{2k_B T A \omega_0 \frac{t_{samp}}{\pi Q}},$$

the noise response is

$$\Delta\theta(\omega) = \tau_{therm}(\omega)R(\omega, \omega_0, A, Q).$$

Setting the signal to noise ratio to 1, the minimum detectible frequency shift is

$$\Delta\omega_0 = \frac{4L}{\lambda t_{samp}} \sqrt{2\pi k_B T A \omega_0 \frac{t_{samp}}{Q}} \min(|(\frac{dR}{d\omega_0})^{-1} R^2(\omega)|),$$

or

$$\frac{\Delta\omega_0}{\omega_0} = \frac{2L}{\lambda} \sqrt{\frac{2k_B T \pi}{A \omega_0^3 t_{samp} Q}}.$$

This unitless noise bound has a simple physical explanation. Using that $\lambda/2L$ is the maximum angle of the driven

cantilever, that $\omega_0 t_{samp}/2\pi$ is averaging time counted in number of oscillations, and that narrower resonances will have less uncertain ω_0 , the noise bound is truly

$$\frac{\Delta\omega_0}{\omega_0} = \sqrt{\frac{\text{Thermal Energy}}{\text{Driven Energy} * \text{Time in Oscillations} * Q}}.$$

Finally, using Equations 6 and 2,

$$\delta\sigma_{xy} = \frac{4L \ln(r_o/r_i)}{\lambda(r_o^2 - r_i^2)VB} \sqrt{\frac{2k_B T A \omega_0}{\pi t_{samp} Q}}.$$

The theoretical uncertainty bound can be compared to the present dummy cantilever data. Calculating A by observing the response magnitude to a known drive and using the vibrational temperature from equipartition along with Equation 10, the best possible fractional uncertainty for such an experiment should be $\sim 10^{-11}$. The fractional uncertainty without vibration isolation is currently $\sim 10^{-9}$.

-
- [1] N. F. Mott, *The Philosophical Magazine: A Journal of Theoretical Experimental and Applied Physics* **19**, 835 (1969).
- [2] B. I. Shklovskii and A. L. Efros, *Electronic Properties of Doped Semiconductors*, 1st ed. (Springer-Verlag, Berlin Heidelberg, 1976).
- [3] M. Steiner and A. Kapitulnik, *Physica C: Superconductivity* **422**, 16 (2005).
- [4] G. Sambandamurthy, L. Engel, A. Johansson, and D. Shahar, *Physical review letters* **92**, 107005 (2004).
- [5] M. A. Paalanen, A. F. Hebard, and R. R. Ruel, *Phys. Rev. Lett.* **69**, 1604 (1992).
- [6] M. P. A. Fisher, *Phys. Rev. Lett.* **65**, 923 (1990).
- [7] Y. Cao, V. Fatemi, A. Demir, S. Fang, S. L. Tomarken, J. Y. Luo, J. D. Sanchez-Yamagishi, K. Watanabe, T. Taniguchi, E. Kaxiras, *et al.*, *Nature* **556**, 80 (2018).
- [8] P. F. Hopkins, M. J. Burns, A. J. Rimberg, and R. M. Westervelt, *Phys. Rev. B* **39**, 12708 (1989).
- [9] D. W. Koon and T. G. Castner, *Phys. Rev. B* **41**, 12054 (1990).
- [10] L. Friedman and M. Pollak, *Philosophical Magazine B* **44**, 487 (1981), <https://doi.org/10.1080/01418638108222584>.
- [11] Y. M. Galperin, E. P. German, and V. G. Karpov, *Zhurnal Eksperimentalnoi I Teoreticheskoi Fiziki* **99**, 343 (1991).
- [12] P. Lou and T. Xiang, arXiv e-prints, cond-mat/0501307 (2005), arXiv:cond-mat/0501307 [cond-mat.mes-hall].
- [13] R. B. Laughlin, *Phys. Rev. B* **23**, 5632 (1981).
- [14] O. M. Von Corbino, *Phys. Z.* **12**, 561 (1911).
- [15] M. Perfetti, *Coordination Chemistry Reviews* **348**, 171 (2017).
- [16] J. Chiaverini, K. Yasumura, and A. Kapitulnik, *Phys. Rev. B* **64**, 014516 (2001).
- [17] A. C. Bleszynski-Jayich, W. E. Shanks, B. Peaudecerf, E. Ginossar, F. von Oppen, L. Glazman, and J. G. E. Harris, *Science* **326**, 272 (2009), <http://science.sciencemag.org/content/326/5950/272.full.pdf>.
- [18] E. Finot, A. Passian, and T. Thundat, *Sensors* **8**, 3497 (2008).
- [19] N. P. Breznay, M. A. Steiner, S. A. Kivelson, and A. Kapitulnik, *PNAS* **113**, 280 (2016), <https://www.pnas.org/content/113/2/280.full.pdf>.
- [20] F. Kurdesau, G. Khripunov, A. D. Cunha, M. Kaelin, and A. Tiwari, *Journal of Non-Crystalline Solids* **352**, 1466–1470 (2006).